

Search for Charged Current Coherent Pion Production on Carbon in a Few-GeV Neutrino Beam

K. Hiraide,¹⁰ J. L. Alcaraz-Aunion,¹ S. J. Brice,⁴ L. Bugel,¹³ J. Catala-Perez,¹⁸ G. Cheng,³ J. M. Conrad,¹³ Z. Djurcic,³ U. Dore,¹⁵ D. A. Finley,⁴ A. J. Franke,³ C. Giganti*,¹⁵ J. J. Gomez-Cadenas,¹⁸ P. Guzowski,⁶ A. Hanson,⁷ Y. Hayato,⁸ G. Jover-Manas,¹ G. Karagiorgi,¹³ T. Katori,⁷ Y. K. Kobayashi,¹⁷ T. Kobilarcik,⁴ H. Kubo,¹⁰ Y. Kurimoto,¹⁰ W. C. Louis,¹¹ P. F. Loverre,¹⁵ L. Ludovici,¹⁵ K. B. M. Mahn,³ C. Mariani[†],¹⁵ S. Masuike,¹⁷ K. Matsuoka,¹⁰ W. Metcalf,¹² G. Mills,¹¹ G. Mitsuka,⁹ Y. Miyachi,¹⁷ S. Mizugashira,¹⁷ C. D. Moore,⁴ Y. Nakajima,¹⁰ T. Nakaya,¹⁰ R. Napor,¹⁴ P. Nienaber,¹⁶ V. Nguyen,¹³ D. Orme,¹⁰ M. Otani,¹⁰ A. D. Russell,⁴ F. Sanchez,¹ M. H. Shaevitz,³ T.-A. Shibata,¹⁷ M. Sorel,¹⁸ R. J. Stefanski,⁴ H. Takei,¹⁷ H.-K. Tanaka,³ M. Tanaka,⁵ R. Tayloe,⁷ I. J. Taylor,⁶ R. J. Tesarek,⁴ Y. Uchida,⁶ R. Van de Water,¹¹ J. J. Walding,⁶ M. O. Wascko,⁶ H. White,⁴ M. J. Wilking,² M. Yokoyama,¹⁰ G. P. Zeller,¹¹ and E. D. Zimmerman²

(The SciBooNE Collaboration)

¹*Institut de Fisica d'Altes Energies, Universitat Autònoma de Barcelona, E-08193 Bellaterra (Barcelona), Spain*

²*Department of Physics, University of Colorado, Boulder, Colorado 80309, USA*

³*Department of Physics, Columbia University, New York, NY 10027, USA*

⁴*Fermi National Accelerator Laboratory; Batavia, IL 60150, USA*

⁵*High Energy Accelerator Research Organization (KEK), Tsukuba, Ibaraki 305-0801, Japan*

⁶*Department of Physics, Imperial College London, London SW7 2AZ, UK*

⁷*Department of Physics, Indiana University, Bloomington, IN 47405, USA*

⁸*Kamioka Observatory, Institute for Cosmic Ray Research, University of Tokyo, Gifu 506-1205, Japan*

⁹*Research Center for Cosmic Neutrinos, Institute for Cosmic Ray*

Research, University of Tokyo, Kashiwa, Chiba 277-8582, Japan

¹⁰*Department of Physics, Kyoto University, Kyoto 606-8502, Japan*

¹¹*Los Alamos National Laboratory; Los Alamos, NM 87545, USA*

¹²*Department of Physics and Astronomy, Louisiana State University, Baton Rouge, LA 70803, USA*

¹³*Department of Physics, Massachusetts Institute of Technology, Cambridge, MA 02139, USA*

¹⁴*Department of Chemistry and Physics, Purdue University Calumet, Hammond, IN 46323, USA*

¹⁵*Universita di Roma La Sapienza, Dipartimento di Fisica and INFN, 1-000185 Rome, Italy*

¹⁶*Physics Department, Saint Mary's University of Minnesota, Winona, MN 55987, USA*

¹⁷*Department of Physics, Tokyo Institute of Technology, Tokyo 152-8551, Japan*

¹⁸*Instituto de Fisica Corpuscular, Universidad de Valencia and CSIC, E-46071 Valencia, Spain*

(Dated: January 10, 2018)

The SciBooNE Collaboration has performed a search for charged current coherent pion production from muon neutrinos scattering on carbon, $\nu_\mu {}^{12}\text{C} \rightarrow \mu {}^{-12}\text{C}\pi^+$, with two distinct data samples. No evidence for coherent pion production is observed. We set 90% confidence level upper limits on the cross section ratio of charged current coherent pion production to the total charged current cross section at 0.67×10^{-2} at mean neutrino energy 1.1 GeV and 1.36×10^{-2} at mean neutrino energy 2.2 GeV.

PACS numbers: 13.15.+g, 13.60.Le, 25.30.Pt, 95.55.Vj

I. INTRODUCTION

Although they have been studied for decades, neutrino-nucleus cross sections between 100 MeV and 10 GeV energy are still known with very poor accuracy. The demand for precise cross section measurements in this energy regime is driven by the needs of the next generation of neutrino oscillation experiments in their pursuit of sub-leading flavor oscillation and charge-parity violation

[1, 2]. Several interaction channels contribute to the total neutrino-nucleus cross section in the neutrino energy range of a few GeV. Interactions producing single pions (charged or neutral) account for a large cross section fraction, which must be understood because they form significant backgrounds for neutrino oscillation searches.

It has been known for years that neutrinos can produce pions by interacting *coherently* with the nucleons forming the target nucleus. The cross section for this process is expected to be smaller than incoherent pion production, the latter being dominated by neutrino-induced baryonic resonance excitation off a single nucleon bound in a nucleus. Moreover, coherent pion production is comparatively poorly understood, although it is characterized by a distinct signature consisting of a nucleus left in the ground state (no nuclear breakup occurs) and a forward

*Present address: DSM/Irfu/SPP, CEA Saclay, F-91191 Gif-sur-Yvette, France

[†]Present address: Department of Physics, Columbia University, New York, NY 10027, USA

scattered pion. Both charged current and neutral current coherent modes are possible, $\nu_\mu A \rightarrow \mu^- A \pi^+$ and $\nu_\mu A \rightarrow \nu_\mu A \pi^0$, where A is a nucleus.

Several theoretical models describing coherent pion production have been proposed, using different formalisms to describe the relevant physics. A first class of models is built on the basis of Adler's PCAC theorem [3], relating the neutrino-nucleus cross section to that of a pion interacting with a nucleus at $Q^2 = 0$; the extrapolation to $Q^2 \neq 0$ is performed via a propagator term [4, 5, 6, 7, 8]. A second commonly-used formalism is based on the description of the coherent production of Δ resonances on nuclei by using a modified Δ -propagator and a distorted wave-function for the pion [9, 10, 11, 12]. While the relationship between neutral current and charged current modes, and that between neutrino and antineutrino coherent pion production cross sections, are relatively well known, order-of-magnitude variations on absolute coherent pion production cross sections are expected within these models. In addition, the cross section dependence on neutrino energy and on target material is also uncertain. It is therefore imperative that more experimental input on coherent pion production in neutrino-nucleus interactions is gathered in the near future.

Coherent pion production in neutrino-nucleus interactions has already been the subject of several experimental campaigns. The neutrino energy range between 1 and 100 GeV has been investigated, including both the charged current and neutral current modes, and using both neutrino and antineutrino probes. A result that has drawn much attention in the neutrino physics community has been the recent non-observation of charged current coherent pion production by the K2K experiment with a 1.3 GeV wide-band neutrino beam [13]. This is motivated by the fact that the K2K Collaboration has quoted an upper limit for the ratio of the charged current coherent pion production cross section to the charged current inclusive cross section that is well below the prediction of the original Rein-Sehgal model [5] that has been adopted in the past to describe coherent pion production processes. In addition, even within more recently proposed models, it is often difficult to reconcile this new and accurate null result at low energies with previous measurements. On the one hand, evidence for neutral current coherent pion production in a neutrino energy range that is similar to K2K has been unambiguously reported from the Aachen-Padova [14] and Gargamelle experimental data [15] first, and more recently also by the MiniBooNE Collaboration [16]. On the other hand, while no measurements of charged current coherent pion production other than the K2K one exist in a similar neutrino energy range, there exist charged current coherent pion production positive results at higher energies (7-100 GeV neutrino energy) from the SKAT [17], CHARM [18], BEBC [19, 20], and FNAL E632 [21] experiments.

In this paper, we discuss the first measurement of charged current coherent pion production by neutrinos

in the SciBooNE experiment [22]. This is a particularly interesting test of the K2K null result, probing a similar neutrino energy range and same target material. Also, compared to K2K, SciBooNE's result presented here is based on a higher-statistics data sample and uses an improved analysis, as will be described below.

This paper is organized as follows. Section II describes the neutrino beam-line and the neutrino flux simulation. The simulation of neutrino interactions with nuclei are described in Section III. The detector configuration and simulation are described in Section IV. A summary of the data set and experimental performance is given in Section V. The data analysis, including the event selection and Monte Carlo (MC) tuning, is described in detail in Section VI. The results of the analysis and discussion are presented along with a summary of systematic uncertainties in Section VII, and the final conclusions are given in Section VIII.

II. NEUTRINO BEAM

The SciBooNE detector has been exposed to the Booster Neutrino Beam (BNB) located at Fermilab. The BNB is a high-intensity, conventional neutrino beam which has been serving the MiniBooNE experiment since 2002.

A. Beam-line Description

The primary beam uses protons accelerated to 8 GeV kinetic energy by the Fermilab Booster. Selected batches containing approximately $4\text{-}5 \times 10^{12}$ protons are extracted and bent toward the BNB target hall via dipole magnets. Each spill is composed of 81 bunches of protons, approximately 6 ns wide each and 19 ns apart, for a total spill duration of 1.6 μs .

Beam proton trajectories and positions are monitored on a pulse-by-pulse basis. The typical beam alignment and divergence measured by the beam position monitors located near the target are within 1 mm and 1 mrad of the nominal target center and axis direction, respectively; the typical beam focusing on target measured by beam profile monitors is of the order of 1-2 mm (RMS) in both the horizontal and vertical directions. These parameters are well within the experiment requirements. The number of protons delivered to the BNB target is measured for each proton batch using two toroids located near the target along the beam-line. The toroid calibration, performed on a pulse-by-pulse basis, provides a measurement of the number of protons to BNB with a 2% accuracy.

Primary protons from the 8 GeV beamline strike a thick beryllium target located in the BNB target hall. Hadronic interactions of the protons with the target material produce a beam of secondary mesons (pions and kaons). The target is made of seven cylindrical slugs for

a total target length of 71.1 cm, or about 1.7 inelastic interaction lengths.

The beryllium target is surrounded by a magnetic focusing horn, bending and sign-selecting the secondary particles that emerge from the interactions in the target along the direction pointing to the SciBooNE detector. The focusing is produced by the toroidal magnetic field present in the air volume between the horn's two coaxial conductors made of aluminum alloy. The horn current pulse is approximately a half-sinusoid of amplitude 174 kA, 143 μ s long, synchronized to each beam spill. The polarity of the horn current flow can be (and has been) switched, in order to focus negatively-charged mesons, and therefore produce an antineutrino instead of a neutrino beam.

The beam of focused, secondary mesons emerging from the target/horn region is further collimated via passive shielding, and allowed to decay into neutrinos in a cylindrical decay region filled with air at atmospheric pressure, 50 m long and 90 cm in radius. A beam absorber located at the end of the decay region stops the hadronic and muonic component of the beam, and only a pure neutrino beam pointing toward the detector remains, mostly from $\pi^+ \rightarrow \mu^+ \nu_\mu$ decays.

B. Neutrino Flux Prediction

Neutrino flux predictions at the SciBooNE detector location are obtained via a GEANT4-based [23] beam Monte Carlo simulation. The same simulation code developed by the MiniBooNE Collaboration is used [24].

In the simulation code, a realistic description of the geometry and materials present in the BNB target hall and decay region is used. Primary protons are generated according to the expected beam optics properties upstream of the target. The interactions of primary protons with the beryllium target are simulated according to state-of-the-art hadron interaction data. Of particular importance for this analysis is π^+ production in proton-beryllium interactions, which uses experimental input from the HARP [25] and BNL E910 [26] experiments. Production of secondary protons, neutrons, charged pions, and charged and neutral kaons is taken into account, and elastic and quasi-elastic scattering of protons in the target are also simulated. Particles emanating from the primary proton-beryllium interaction in the target are then propagated within the GEANT4 framework, which accounts for all relevant physics processes. Hadronic reinteractions of pions and nucleons with beryllium and aluminum materials are particularly important and are described by custom models, while other hadronic processes and all electromagnetic processes (energy loss, multiple scattering, effect of horn magnetic field, etc.) are described according to default GEANT4 physics lists. A second, FORTRAN-based Monte Carlo code uses the output of the GEANT4 program as input, and is responsible for generating the neutrino kinematics distributions

from meson and muon decays, and for obtaining the final neutrino fluxes extrapolated to the SciBooNE detector with negligible beam Monte Carlo statistical errors. Current best knowledge of neutrino-producing meson and muon decay branching fractions, and decay form factors in three-body semi-leptonic decays, are used. Polarization effects in muon decays are also accounted for.

Once produced by the simulation, neutrinos are extrapolated along straight lines toward the SciBooNE detector. All neutrinos whose ray traces cross any part of the detector volume are considered for SciBooNE flux predictions. Based on accurate survey data, the distance between the center of the beryllium target and the center of the SciBar detector is taken to be 99.9 m, with the SciBooNE detector located on beam axis within a tolerance of a few cm. Each simulated neutrino interaction is linked to its detailed beam information and history, which includes neutrino flavor, energy, parent type and kinematics, and ray trace entry and exit points within the detector volume; the ray trace information is used to determine the incoming neutrino's direction and interaction location. Proper weights for each beam neutrino event are computed, using this beam neutrino information, as well as information from the interaction and detector simulation: neutrino interaction probability, and detailed SciBooNE detector geometry and specifications.

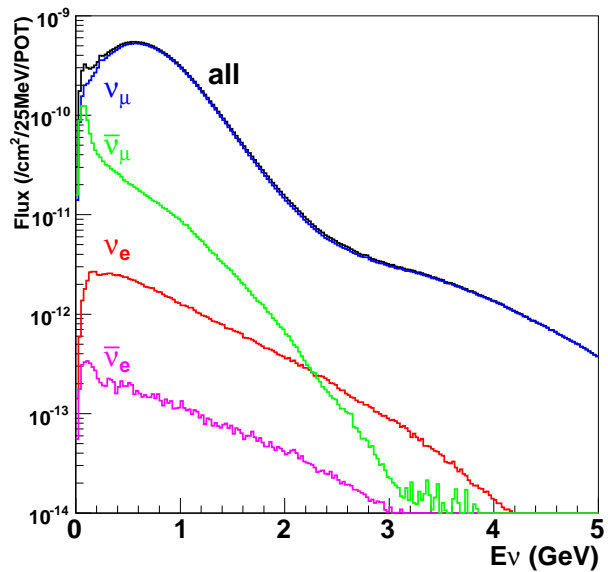


FIG. 1: Neutrino flux prediction at the SciBooNE detector as a function of neutrino energy E_ν , normalized per unit area, proton on target (POT) and neutrino energy bin width. The spectrum is averaged within 2.12 m from the beam center. The total flux and contributions from individual neutrino flavors are shown.

The neutrino flux prediction at the SciBooNE detector location and as a function of neutrino energy is shown

in Fig. 1. A total neutrino flux per proton on target of $2.2 \times 10^{-8} \text{ cm}^{-2}$ is expected at the SciBooNE detector location and in neutrino running mode (positive horn polarity), with a mean neutrino energy of 0.7 GeV. The flux is dominated by muon neutrinos (93% of total), with small contributions from muon antineutrinos (6.4%), and electron neutrinos and antineutrinos (0.6% in total). For the neutrino flux predictions used in this analysis, no information from BNB (SciBooNE or MiniBooNE) neutrino data is used as experimental input.

III. NEUTRINO INTERACTION SIMULATION

The neutrino interactions with nuclear targets are simulated with the NEUT program library [27, 28] which is used in the Kamiokande, Super-Kamiokande, K2K, and T2K experiments. NEUT handles protons, oxygen, carbon, and iron as nuclear targets in the energy range from 100 MeV to 100 TeV. In NEUT, the following neutrino interactions in both neutral and charged currents are simulated: quasi-elastic scattering ($\nu N \rightarrow \ell N'$), single meson production ($\nu N \rightarrow \ell N' m$), single gamma production ($\nu N \rightarrow \ell N' \gamma$), coherent π production ($\nu^{12}\text{C}(\text{or } ^{56}\text{Fe}) \rightarrow \ell \pi^{12}\text{C}(\text{or } ^{56}\text{Fe})$), and deep inelastic scattering ($\nu N \rightarrow \ell N' \text{hadrons}$), where N and N' are the nucleons (proton or neutron), ℓ is the lepton, and m is the meson. Following the primary neutrino interactions in nuclei, re-interactions of the mesons and hadrons with the nuclear medium are also simulated.

A. Coherent π production

The signal for this analysis, coherent pion production, is a neutrino interaction with a nucleus which remains intact, releasing one pion with the same charge as the incoming weak current. Because of the small momentum transfer to the target nucleus the outgoing lepton and pion tend to go in the forward direction (in the lab frame). The formalism developed by Rein and Sehgal [5] is used to simulate the interactions, including the recent correction of lepton mass effects [8]. The axial vector mass, M_A , is set to $1.0 \text{ GeV}/c^2$. The nuclear radius parameter R_0 is set to 1.0 fm. For the total and inelastic pion-nucleon cross sections used in the formalism, the fitted results given in Rein and Sehgal's paper are employed. The total cross section on ^{12}C is shown in Fig. 2, with comparisons of other models discussed in the introduction. The Rein and Sehgal model predicts charged current coherent pion production to be approximately 1% of the total neutrino interactions in SciBooNE.

B. Quasi-elastic scattering

The dominant interaction in the SciBooNE neutrino energy range is quasi-elastic scattering, which is imple-

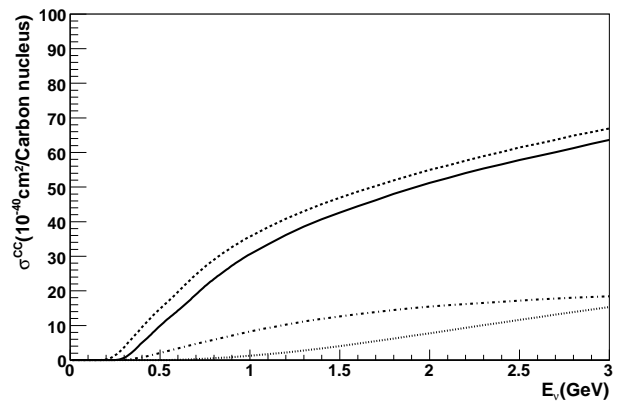


FIG. 2: Cross section for $\nu_{\mu}^{-} {}^{12}\text{C} \rightarrow \mu^{-} \pi^{+} {}^{12}\text{C}$ interaction. The solid line represents the Rein and Sehgal model with lepton mass effects [8] (the default model of the signal for this analysis), the dashed line represents the Rein and Sehgal model without lepton mass effects [5], the dotted line represents the model of Kartavtsev *et al.* [7], and the dashed-dotted line represents the model of Alvarez-Ruso *et al.* [11]. The model of Singh *et al.* [9] gives a cross section similar to the model of Alvarez-Ruso *et al.*

mented using the model of Llewellyn-Smith [29]. For scattering off nucleons in the nucleus, we use the relativistic Fermi gas model of Smith and Moniz [30]. The nucleons are treated as quasi-free particles and the Fermi motion of nucleons along with the Pauli exclusion principle is taken into account. The momentum distribution of the target nucleon is assumed to be flat up to a fixed Fermi surface momentum of $217 \text{ MeV}/c$ for carbon and $250 \text{ MeV}/c$ for iron. The same Fermi momentum distribution is also used for all of the other nuclear interactions. The nuclear potential is set to 27 MeV for carbon and 32 MeV for iron. Both vector and axial-vector form factor are assumed to be dipole. The vector mass in quasi-elastic scattering is set to be $0.84 \text{ GeV}/c^2$. The axial vector mass, M_A , is set to be $1.21 \text{ GeV}/c^2$ as suggested by recent results [31, 32].

C. Single meson production via baryon resonances

The second most probable interaction in SciBooNE is the resonant single meson production of π , K , and η described by the model of Rein and Sehgal [33]. The model assumes an intermediate baryon resonance, N^* , in the reaction of $\nu N \rightarrow \ell N^*$, $N^* \rightarrow N' m$. The differential cross section of single meson production depends on the amplitude for the production of a given resonance and the probability of the baryon resonance decay to the meson. All intermediate baryon resonances with mass less than $2 \text{ GeV}/c^2$ are included. Those baryon resonances with mass greater than $2 \text{ GeV}/c^2$ are simulated as deep inelastic scattering. Lepton mass effects from the non-conservation of lepton current and the pion-pole term in the hadronic axial vector current are included in the

simulation [34, 35].

To determine the angular distribution of a pion in the final state, Rein's method [36] is used for the $P_{33}(1232)$ resonance. For other resonances, the directional distribution of the generated pion is set to be isotropic in the resonance rest frame. The angular distribution of π^+ has been measured for $\nu_\mu p \rightarrow \mu^- p \pi^+$ [37] and the results agree well with NEUT's prediction. Pauli blocking is accounted for in the decay of the baryon resonance by requiring the momentum of the nucleon to be larger than the Fermi surface momentum. Pion-less Δ decay is also taken into account, where 20% of the events do not have a pion and only the lepton and nucleon are generated [38]. The axial vector mass, M_A , is set to be $1.21 \text{ GeV}/c^2$.

D. Deep inelastic scattering

The cross section for deep inelastic scattering (DIS) is calculated using the GRV98 parton distribution functions [39]. Additionally, we have included the corrections in the small Q^2 region developed by Bodek and Yang [40]. In the calculation, the hadronic invariant mass, W , is required to be larger than $1.3 \text{ GeV}/c^2$. Also, the multiplicity of pions is restricted to be larger than or equal to two for $1.3 < W < 2.0 \text{ GeV}/c^2$, because single pion production is already included in the simulation, as described above. The multi-hadron final states are simulated with two models: a custom-made program [41] for the event with W between 1.3 and $2.0 \text{ GeV}/c^2$ and PYTHIA/JETSET [42] for the events with W larger than $2 \text{ GeV}/c^2$.

E. Intra-nuclear interactions

The intra-nuclear interactions of mesons and nucleons produced in neutrino interactions in the nuclei are simulated. These interactions are treated using a cascade model, and each of the particles is traced until it escapes from the nucleus.

Among all the interactions of mesons and nucleons, the interactions of pions are most important to this analysis. The inelastic scattering, charge exchange and absorption of pions in the nuclei are simulated. The interaction cross sections of pions in the nuclei are calculated using the model by Salcedo *et al.* [43], which agrees well with past experimental data [44]. If inelastic scattering or charge exchange occurs, the direction and momentum of pions are determined by using results from a phase shift analysis of pion-nucleus scattering experiments [45]. When calculating the pion scattering amplitude, Pauli blocking is taken into account by requiring the nucleon momentum after the interaction to be larger than the Fermi surface momentum at the interaction point.

Re-interactions of the recoil protons and neutrons produced in neutrino interactions are also important, because the proton tracks are used to classify the neutrino

event type. Nucleon-nucleon interactions modify the outgoing nucleon's momentum and direction. Both elastic scattering and pion production are considered. In order to simulate these interactions, a cascade model is again used and the generated particles in the nucleus are tracked using the same code as for the mesons.

No de-excitation gamma-ray from the carbon nucleus is simulated when nuclear breakup occurs.

IV. NEUTRINO DETECTOR

The SciBooNE detector is located 100 m downstream from the beryllium target on the axis of the beam. The detector comprises three sub-detectors: a fully active and finely segmented scintillator tracker (SciBar), an electromagnetic calorimeter (EC), and a muon range detector (MRD).

A. Detector Description

Fig. 3 shows an event display of a typical muon neutrino charged current single charged pion event candidate. Detector coordinates are shown in the figure. SciBooNE uses a right-handed Cartesian coordinate system in which the z axis is the beam direction and the y axis is the vertical upward direction. The origin is located on the most upstream surface of SciBar in the z dimen-

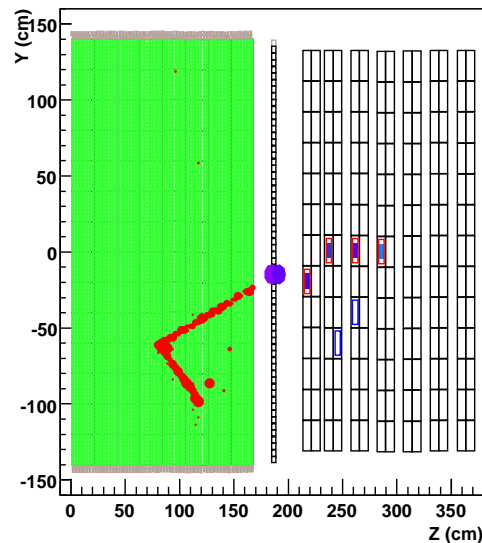


FIG. 3: Event display of a typical muon neutrino charged current single charged pion event candidate in SciBooNE data. The neutrino beam runs from left to right in this figure, encountering SciBar, the EC and MRD, in that order. The circles on SciBar and the EC indicate ADC hits for which the area of the circle is proportional to the energy deposition in that channel. Filled boxes in the MRD show ADC hits in time with the beam window.

sion, and at the center of the SciBar scintillator plane in the x and y dimensions. Since each sub-detector is read out both vertically and horizontally, two views are defined; the top view (z - x projection) and the side view (z - y projection).

The SciBar detector [46] is positioned upstream of the other sub-detectors. The primary role of SciBar is to reconstruct the neutrino-nucleus interaction vertex and detect charged particles produced by neutrino interactions. Moreover, SciBar is capable of particle identification based on deposited energy. SciBar was designed and built as a near detector for the K2K experiment. After K2K's completion, SciBar was relocated to the Fermilab BNB for SciBooNE.

SciBar consists of 14,336 extruded plastic scintillator strips which serve as the target for the neutrino beam as well as the active detection medium. Originally produced by Fermilab, each strip has a dimension of $1.3 \times 2.5 \times 300$ cm³. The scintillators are arranged vertically and horizontally to construct a $3 \times 3 \times 1.7$ m³ volume with a total mass of 15 tons. Each strip is read out by a wavelength shifting (WLS) fiber attached to a 64-channel multi-anode PMT. Charge and timing information from each PMT is recorded by front-end electronics boards (FEB) attached directly to the PMT and a back-end VME module [47]. The FEB uses VA/TA ASICs; the VA handles charge information from the PMT with a 32-channel preamplifier chip with a shaper and multiplexer, while the TA provides timing information by taking the logical "OR" of 32 channels. The charge and timing information are digitized by ADC and multi-hit TDC modules on back-end electronics, and read out through the VME bus.

The gains of all PMT channels were measured prior to installation in K2K. SciBar is equipped with a gain calibration system comprised of LEDs to monitor and correct gain drift during the data taking; the gain stability is monitored with precision better than 1%. Cosmic ray data are also employed to calibrate the PMT gains and scintillator light yield, including attenuation of the WLS-fibers. These calibration data, LED and cosmic, are taken between beam spills and continuously monitored. Calibration data verify the light yield was stable within 1% during operation. The timing resolution for minimum-ionizing particles was evaluated with cosmic ray data to be 1.6 ns. The average light yield for minimum-ionizing particles is approximately 20 photoelectrons per 1.3 cm path length, and the typical pedestal width is below 0.3 photoelectron. The hit finding efficiency evaluated with cosmic ray data is more than 99.8%. The minimum length of a reconstructable track is approximately 8 cm (three layers hit in each view). The track finding efficiency for single tracks of 10 cm or longer is more than 99%.

The EC is located just downstream of SciBar, and is designed to measure the electron neutrino contamination in the beam and tag photons from π^0 decay. The EC is a "spaghetti" type calorimeter comprised of 1 mm di-

ameter scintillating fibers embedded in lead foil. The calorimeter is made of modules of dimensions $262 \times 8 \times 4$ cm³. Each module is read out by two green-extended 1 inch Hamamatsu PMTs per side, 256 PMTs total. The modules were originally built for the CHORUS neutrino experiment at CERN [48] and later used in HARP and then K2K. The modules construct one vertical and one horizontal plane, and each plane has 32 modules. The EC has a thickness of 11 radiation lengths along the beam direction. The planes cover an active area of 2.7×2.6 m².

The charge information from each PMT is recorded. A minimum ionizing particle with a minimal path length deposits approximately 91 MeV in the EC. The energy resolution for electrons was measured to be $14\%/\sqrt{E}$ (GeV) using a test beam [48].

The MRD is installed downstream of the EC and is designed to measure the momentum of muons produced by charged-current neutrino interactions. The MRD was constructed for SciBooNE at Fermilab, primarily out of parts recycled from past experiments. It has 12 iron plates with thickness of 5 cm which are sandwiched between planes of 6 mm thick scintillation counters, 13 alternating horizontal and vertical planes, which are read out via 2 inch PMTs from a variety of past experiments; there are 362 PMTs total. Each iron plate covers an area of 274×305 cm². The total mass of absorber material is approximately 48 tons. The MRD measures the momentum of muons up to 1.2 GeV/ c using the observed muon range. Charge and timing information from each PMT are recorded. Hit finding efficiency was continuously monitored using cosmic ray data taken between beam spills; the average hit finding efficiency is 99%.

SciBooNE has two global triggers, the beam trigger and the off-beam trigger. Two types of data are collected in one beam cycle, neutrino data with the beam trigger and calibration data with the off-beam trigger. One cycle is about 2 sec which is defined by the accelerator timing sequence. The BNB receives one train of proton beam pulses per cycle, with a maximum of 10 pulses in a row at 15 Hz.

A fast timing signal sent by the extraction magnet on BNB pulses establishes a beam-trigger. Once the beam trigger condition is set, all sub-detector systems read out all channels irrespective of hit occupancy (i.e. whether or not a neutrino interaction occurred), ensuring unbiased neutrino data.

After the beam trigger turns off, the off-beam trigger condition is automatically set and each sub-detector takes calibration data. There are three types of calibration data: pedestal, LED (only for SciBar) and cosmic ray data. The pedestal and LED data are collected once per cycle. For cosmic ray data, there are two independent trigger blocks: SciBar/EC and MRD. SciBar and the EC use a common cosmic ray trigger which is generated using fast signals from the TA. The MRD has its own cosmic ray trigger which is also self-generated by discriminator outputs. Both SciBar/EC and the MRD collect 20 cosmic ray triggers in a cycle.

B. Detector simulation

The GEANT4 framework is used for the detector simulation. The Bertini cascade model within GEANT4 [49] is used to simulate the interactions of hadronic particles with detector materials. The detector simulation includes a detailed geometric model of the detector, including the detector frame and experimental hall and soil, which is based on survey measurements taken during detector construction.

In the detector simulation of SciBar, low level data parameters are used as input to the simulation whenever possible. The energy loss of a charged particle in a single strip is simulated by GEANT, and this energy scale is tuned using cosmic ray data. Scintillator quenching is simulated using Birk's law [50] with a value of Birk's constant, measured for K2K, of 0.0208 cm/MeV [51]. The energy deposited by a charged particle is converted to photoelectrons using conversion factors measured for each channel with cosmic muons. The measured light attenuation length of each fiber (approximately 350 cm on average) is used in the simulation. Crosstalk between nearby MA-PMT channels is simulated using values measured in a test stand prior to installation. The number of photoelectrons is smeared by Poisson statistics, and the single photoelectron resolution of the MA-PMT is simulated. To simulate the digitization of the PMT signal, the number of photoelectrons is converted to ADC counts, and then electronics noise and threshold effects of the TA are simulated.

TDC hit simulation includes light propagation delays in the WLS fibers. A logical OR of 32 MA-PMT channels is made for each TDC channel, and the time of each hit is converted to TDC counts. Multiple TDC hits in each channel are simulated.

In the EC detector simulation, true energy deposition in scintillating fibers in the detector is converted to the number of photoelectrons using a conversion factor which is measured for each channel with cosmic-ray muons. The attenuation of light in the fiber is simulated using the measured attenuation length value. The number of photoelectrons is smeared by Poisson statistics and by the PMT resolution, and then converted to ADC counts. The time-dependent ADC gain due to the overshoot of the PMT signal is simulated based on a measurement with cosmic muons. Electronics noise is also simulated.

For the detector simulation of the MRD, true energy deposition in each scintillator is converted to ADC counts using the conversion factor measured with cosmic muons. The attenuation of light in the scintillator as well as electronics noise are simulated. Gaps between scintillator counters in each plane, which cause inefficiency, are included in the simulation. The time of energy deposition is digitized and converted into TDC counts.

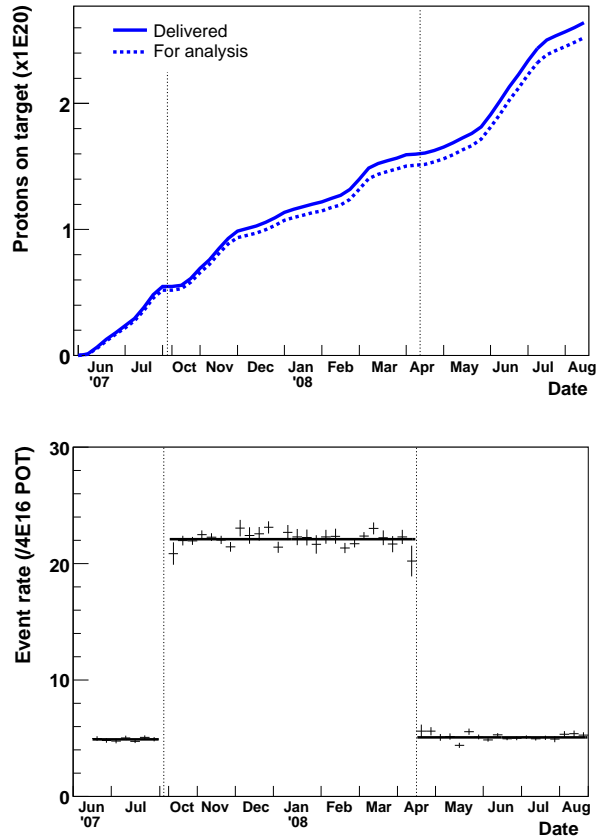


FIG. 4: Experimental performance. In the top panel, the solid line shows the history of the accumulated number of protons on target and the dashed line shows the number of protons on target passing all data quality cuts. The bottom panel shows the number of charged current candidate events in SciBar normalized to the number of protons on target. The event rate difference between neutrino and antineutrino modes can be seen clearly.

V. DATA SUMMARY

The SciBooNE experiment took data from June 2007 until August 2008. The data-taking is divided into three periods depending on the polarity of the horn, as summarized in Table I. Fig. 4(top) shows a history of the accumulated number of protons on target; the two curves show the total protons on target for all events and the protons on target for events passing all data quality cuts, described below.

In total, 2.64×10^{20} protons on target were delivered to the beryllium target during the SciBooNE data run. The beam datastream (measuring, for example, magnet current settings, measured beam intensity, measured peak horn current) is synchronized and merged with the corresponding SciBooNE detector datastream, provided that the spill time as measured by the beam instrumentation and by the detector match within 10 ms of each other.

TABLE I: Summary of SciBooNE data-taking. The table shows the number of protons on target (POT) collected after application of data quality cuts, as described in the text.

| Run | Period | POT |
|----------------------|-----------------------|-----------------------|
| Run 1 (Antineutrino) | Jun. 2007 - Aug. 2007 | 0.52×10^{20} |
| Run 2 (Neutrino) | Oct. 2007 - Apr. 2008 | 0.99×10^{20} |
| Run 3 (Antineutrino) | Apr. 2008 - Aug. 2008 | 1.01×10^{20} |

Only spills that satisfy certain beam quality cuts are used for analysis. We require that the beam intensity is at least 0.1×10^{12} protons per spill, that the agreement between the two toroid readouts along the beam-line is within 10%, that the absolute peak horn current is greater than 170 kA, and that the targeting efficiency is greater than 95%. Overall, beam quality cuts reject less than 1% of the total number of protons on target accumulated during the run. A somewhat larger fraction of protons on target is rejected because of detector dead time, yielding about a 95% efficiency to satisfy all (beam plus detector) data quality cuts. After all beam and detector quality cuts, 2.52×10^{20} protons on target are usable for physics analyses.

In this analysis, the full neutrino data sample is used, corresponding to 0.99×10^{20} protons on target satisfying all data quality cuts, collected between October 2007 and April 2008. During that time, all detector channels were operational on beam triggers. The experimental stability is demonstrated in Fig. 4(bottom), which shows the number of charged current event candidates per protons on target. In this figure, the event reconstruction is a simple χ^2 track finder which is used only for operations related studies, and not for the analysis described in this paper. The figure illustrates the event rate difference between neutrino mode and antineutrino mode running.

The antineutrino data sample collected before and after the neutrino data-taking period is not considered in this analysis.

VI. EVENT RECONSTRUCTION AND ANALYSIS

A. Track Reconstruction

The first step of the event reconstruction is to search for two-dimensional tracks in each view of SciBar using a cellular automaton algorithm [52]. For tracking, the hit threshold is set to two photoelectrons, corresponding to approximately 0.2 MeV. Three dimensional tracks are reconstructed by matching the timing and z -edges of the two dimensional tracks. The timing difference between two two dimensional tracks is required to be less than 50 nsec, and the z -edge difference must be less than 6.6 cm for upstream and downstream edges. Reconstructed tracks are required to have at least three-

layer penetration, and therefore the minimum length of a reconstructed track is 8 cm in the beam direction. According to the MC simulation, 96% of charged current interactions in SciBar are reconstructed to have at least one track.

To identify charged current events, we look for events in which at least one reconstructed track in SciBar is matched with a track or hits in the MRD. Such a track is defined as a SciBar-MRD matched track. The most energetic SciBar-MRD matched track in any event is considered as a muon candidate. For matching a MRD track to a SciBar track, the upstream edge of the MRD track is required to be on either one of the first two layers of the MRD. The transverse distance between the two tracks at the first layer of the MRD must be less than 30 cm. The requirement on the difference between track angles with respect to the beam direction is given by $|\theta_{\text{MRD}} - \theta_{\text{SB}}| < \theta_{\text{max}}$, where θ_{max} is a function of the length of the MRD track, varying between 0.4 radian and 1.1 radians. For track reconstruction in the MRD, at least two hit layers in each view are needed, and thus this matching method is used for tracks which penetrate at least three steel plates. If no MRD track is found, we extrapolate the SciBar track to the MRD and search for nearby contiguous hits in the MRD identifying a short muon track. For matching MRD hits to a SciBar track, the MRD hit is required to be within a cone with an aperture of ± 0.5 radian and a transverse offset within 10 cm of the extrapolated SciBar track at the upstream edge of the MRD. The timing difference between the SciBar track and the track or hits in the MRD is required to be within 100 nsec. The matching criteria impose a muon momentum threshold of 350 MeV/ c .

B. Particle Identification

The SciBar detector has the capability to distinguish protons from muons and pions using dE/dx . The particle identification variable, Muon Confidence Level (MuCL) is calculated as follows. The confidence level at each plane is first defined as the fraction of events in the expected dE/dx distribution of muons above the observed value, $(dE/dx)_{\text{obs}}$. The expected dE/dx distribution of muons is obtained by using cosmic-ray muons. Each plane's confidence level is combined to form a total confidence level, assuming the confidence level at each layer is independent. The MuCL is calculated as

$$\text{MuCL} = P \times \sum_{i=0}^{n-1} \frac{(-\ln P)^i}{i!} \quad (1)$$

where n is the number of planes penetrated by the track, $P = \prod_{i=1}^n \text{CL}_i$, CL_i is the confidence level at the i -th plane.

Fig. 5 shows the dE/dx distributions of muon and proton enriched samples. The predicted distributions of true muon and proton tracks are shown as hatched

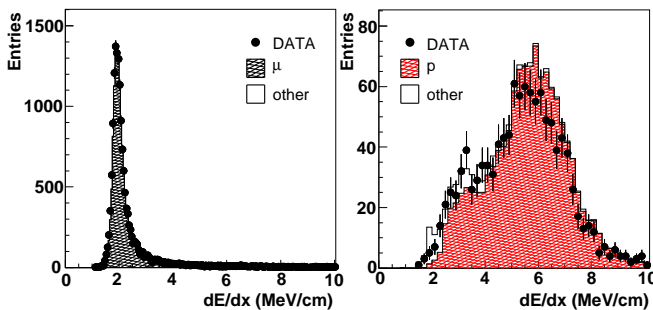


FIG. 5: (Color online) dE/dx of muon enriched sample (left) and proton enriched sample (right).

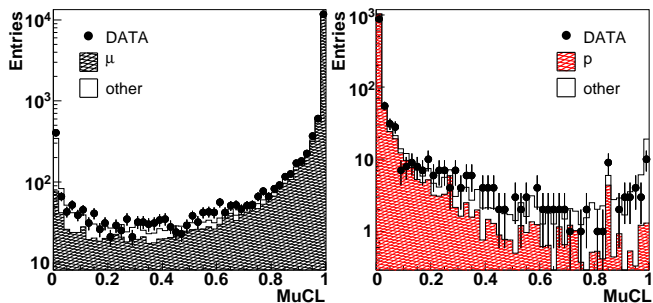


FIG. 6: (Color online) MuCL of muon enriched (left) and proton enriched (right) samples.

histograms. To select muon candidates for this study, we first select SciBar-MRD matched tracks. According to the MC simulation, the sample is 94.7% pure muons with a small contamination of protons and charged pions. For proton candidates, we select the second track in a charged current quasi-elastic (CC-QE) scattering enriched sample made by cutting on a kinematic variable described later. The fraction of protons in the sample is 92.1%, estimated with the MC simulation. The contamination of charged pions and muons are estimated to be 5.5% and 1.6%, respectively. Proton candidates are clearly separated from muon candidates.

The MuCL distributions for the muon enriched sample and the proton enriched sample are shown in Fig. 6. Tracks with MuCL greater than 0.05 are considered muon-like (or pion-like) and the others are classified as proton-like. The probability of misidentification is estimated to be 1.1% for muons and 12% for protons, averaged over track length in the muon and proton enriched samples.

C. Charged Current Event Selection

Events with at least one SciBar-MRD matched track are selected as charged current event candidates. We reject events with hits associated with the muon candi-

date on the most upstream layer of SciBar to eliminate incoming particles due to neutrino interactions in the upstream wall or soil. The hit threshold for this veto cut is set to two photoelectrons. The neutrino interaction vertex is reconstructed as the upstream edge of the muon track. The vertex resolution is approximately 0.5 cm in each dimension, estimated with the MC simulation. We select events whose vertices are in the SciBar fiducial volume, defined to be ± 130 cm in both the x and y dimensions, and $2.62 \text{ cm} < z < 157.2 \text{ cm}$, a total mass of 10.6 tons. The background contamination due to neutrino events which occur in the EC and MRD is 2.0% and 0.5%, respectively. Finally, the time of the muon candidate is required to be within a $2 \mu\text{sec}$ window around the beam pulse. The cosmic-ray background contamination in the beam timing window is only 0.5%, estimated using a beam-off timing window. According to the MC simulation, the selection efficiency and purity of true ν_μ charged current events are 27.9% and 92.8%, respectively. Impurity comes from ν_μ neutral current events (3.0%), $\bar{\nu}_\mu$ charged current events (1.6%), and neutrino events which occur in the EC/MRD (2.5%). The average neutrino beam energy for true charged current events in the sample is 1.2 GeV. This SciBar-MRD matched sample is our standard charged current data set and defines the MC normalization, i.e. the MC distributions are normalized to the number of SciBar-MRD matched events in data.

Two sub-samples of the SciBar-MRD matched sample are further defined; the MRD stopped sample and the MRD penetrated sample. Events with the muon stopping in the MRD are classified as MRD stopped events, in which we can measure the muon momentum. Events with the muon exiting from the downstream end of the MRD are defined as the MRD penetrated sample, in which we can measure only a part of the muon momentum. The average neutrino beam energy for true charged current events in the MRD stopped and MRD penetrated samples are 1.0 GeV and 2.0 GeV, respectively, enabling a measurement of charged current coherent pion production at two different mean neutrino energies.

The slopes of the muon angles with respect to the beam in the two SciBar views are used to calculate the three dimensional muon angle with respect to the beam (θ_μ). The kinetic energy of the muon is calculated by the range and expected energy deposition per unit length (dE/dx) in SciBar, the EC and the MRD,

$$\begin{aligned} E_{\text{kin}} &= E^{\text{SB}} + E^{\text{EC}} + E^{\text{MRD}} \\ &= \left. \frac{dE}{dx} \right|_{\text{SB}} L_{\text{SB}} + \frac{\Delta E_0^{\text{EC}}}{\cos \theta_\mu} + E^{\text{MRD}}(L_{\text{MRD}}) \end{aligned} \quad (2)$$

where E^{SB} , E^{EC} , and E^{MRD} are the energy deposition in each detector. L_{SB} and L_{MRD} are the track length of the muon in SciBar and the range in the MRD, respectively. We set $dE/dx|_{\text{SB}}$ to 2.04 MeV/cm, and ΔE_0^{EC} , which is the energy deposited in the EC by a horizontally traversing minimum ionizing particle, is set to 91 MeV,

estimated with the GEANT4 simulation. E^{MRD} is calculated from a range to energy lookup table based on the MC simulation. For muons stopping in the MRD, the average muon momentum and muon angular resolutions are 50 MeV/ c and 0.9 degree, respectively. For muons exiting the MRD, only a lower limit on muon momentum is obtained, while the muon angle is determined with the same resolution as that of stopping muons. The systematic uncertainty in the muon momentum scale is estimated to be 2% which is dominated by the difference among various calculations of the range to energy lookup table.

D. Event Classification

The MRD stopped and MRD penetrated samples are further divided into sub-samples with the same selection criteria. Once the muon candidate and the neutrino interaction vertex are reconstructed, we search for other tracks originating from the vertex. For this purpose, the track edge distance is defined as the 3D distance between the vertex and the closer edge of another reconstructed track. Tracks whose edge distance is within 10 cm are called vertex-matched tracks. Fig. 7 shows the distribution of the number of tracks at the vertex for the MRD stopped sample. For the MC simulation, the contributions from charged current coherent pion, charged current resonant pion, charged current quasi-elastic, and other interactions are shown separately. Most events are reconstructed as either one track or two track events. The two track sample is further divided based on particle identification. We first require that the MuCL of the SciBar-MRD matched track is greater than 0.05 to reject events with a proton penetrating into the MRD. Then the second track in the event is classified as a pion-like or a proton-like track with the same MuCL threshold. Fig. 8 shows the contributions to the second track from true proton, pion, muon, and electron tracks as predicted by the MC simulation.

In a charged current resonant pion event, $\nu p \rightarrow \mu^- p \pi^+$, the proton is often not reconstructed due to its low energy, and such an event is therefore identified as a two track $\mu + \pi$ event. To separate charged current coherent pion events from charged current resonant pion events, additional protons with momentum below the tracking threshold are instead detected by their large energy deposition around the vertex, so-called vertex activity. We search for the maximum deposited energy in a strip around the vertex, an area of 12.5 cm \times 12.5 cm in both views. Fig. 9 shows the maximum energy for $\mu + \pi$ events in the MRD stopped sample. A peak around 6 MeV corresponds to the energy deposited in the strip containing the vertex by two minimum ionizing particles, and a high energy tail is mainly due to the low energy proton. To simulate such protons, we consider re-interactions of nucleons in the nucleus as described in Sec. III E as well as ones outside the nucleus (de-

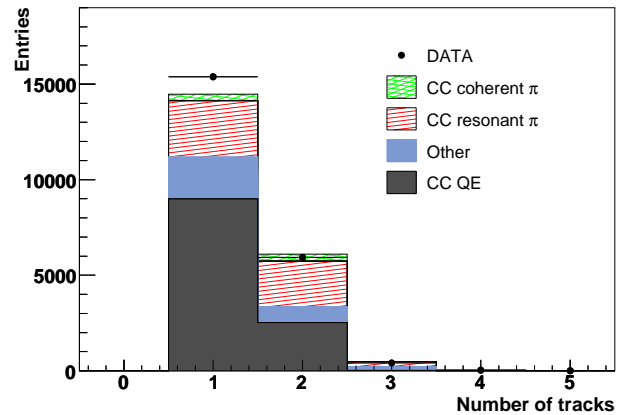


FIG. 7: (Color online) Number of vertex-matched tracks for the MRD stopped sample. The MC distribution shown here is before tuning.

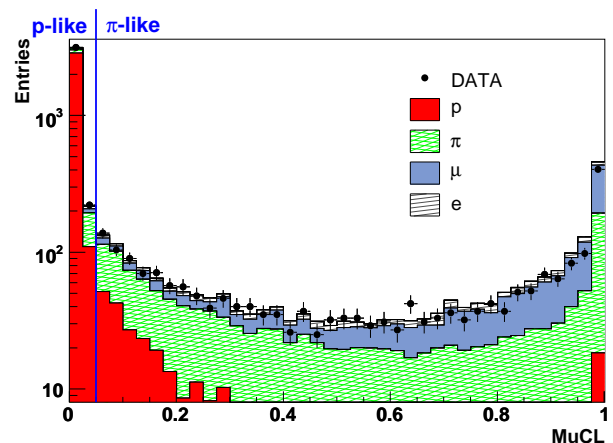


FIG. 8: (Color online) MuCL for the second track in the two-track sample. The MC distribution shown here is before tuning.

scribed in Sec. IV B). De-excitation gamma-rays from the carbon nucleus do not affect the distribution since most of the gamma-rays first interact outside the vertex region. Events with energy deposition greater than 10 MeV are considered to have activity at the vertex. Charged current coherent pion candidates are extracted from the sample of $\mu + \pi$ events without vertex activity. Four sub-samples, the one track events, $\mu + p$ events, $\mu + \pi$ events with vertex activity, and $\mu + \pi$ events without vertex activity in the MRD stopped sample are used for constraining systematic uncertainties in the simulation, described next.

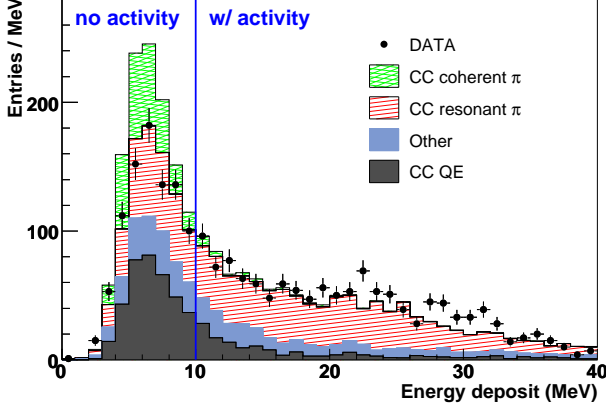


FIG. 9: (Color online) Maximum deposited energy in a strip around the vertex for the $\mu + \pi$ events. The MC distribution shown here is before tuning.

E. Tuning the Monte Carlo Simulation

The MC simulation includes systematic uncertainties due to the detector response, nuclear effects, neutrino interaction models, and neutrino beam spectrum, and these uncertainties affect background estimation. The sources of systematic uncertainty are summarized in Section VII B. In order to constrain these uncertainties, the MC distributions of the square of the four-momentum transfer (Q^2) are fitted to the distributions of the four aforementioned data samples. The reconstructed Q^2 is calculated as

$$Q_{\text{rec}}^2 = 2E_{\nu}^{\text{rec}}(E_{\mu} - p_{\mu} \cos \theta_{\mu}) - m_{\mu}^2 \quad (3)$$

where E_{ν}^{rec} is the reconstructed neutrino energy calculated by assuming charged current quasi-elastic kinematics,

$$E_{\nu}^{\text{rec}} = \frac{1}{2} \frac{(m_p^2 - m_{\mu}^2) - (m_n - V)^2 + 2E_{\mu}(m_n - V)}{(m_n - V) - E_{\mu} + p_{\mu} \cos \theta_{\mu}} \quad (4)$$

where m_p and m_n are the mass of proton and neutron, respectively, and V is the nuclear potential, which is set to 27 MeV. The one track events, $\mu + p$ events, and $\mu + \pi$ events with and without vertex activity are fit simultaneously. Each Q_{rec}^2 distribution is fit in bins of width 0.05 (GeV/c)² up to 1 (GeV/c)².

We introduce eight fitting parameters; the normalization factor of the MRD stopped sample (R_{norm}), the resonant pion scale factor (R_{res}), the scale factor of other non-QE interactions (R_{other}), the ratio of the number of two track events to the number of one track events ($R_{2\text{trk}/1\text{trk}}$), the ratio of the number of $\mu + p$ events to the number of $\mu + \pi$ events ($R_{p/\pi}$), the ratio of the number of low vertex activity $\mu + \pi$ events to the number of high vertex activity $\mu + \pi$ events (R_{act}), the muon momentum

scale (R_{pscale}), and a charged current quasi-elastic Pauli-suppression parameter κ . All parameters are ratios to nominal values in the MC simulation, i.e. all parameters are set to 1 in the default MC simulation.

The parameters $R_{2\text{trk}/1\text{trk}}$, $R_{p/\pi}$, and R_{act} represent possible migrations between subsamples due to systematic uncertainties. The parameter R_{pscale} changes the scale of the reconstructed muon momentum for the MC simulation. The parameter κ , which was first introduced by MiniBooNE [32], controls the strength of Pauli-blocking and thus suppresses low Q^2 charged current quasi-elastic events. We employ this parameter in the fitting because a deficit of data is found at low Q^2 in the one track sample where the charged current quasi-elastic interaction is dominant.

The χ^2 function to be minimized is given by:

$$\chi^2 = \chi_{\text{dist}}^2 + \chi_{\text{sys}}^2. \quad (5)$$

The term χ_{dist}^2 is calculated using a binned likelihood defined as [53]:

$$\begin{aligned} \chi_{\text{dist}}^2 &= -2 \sum_{i,j} \ln \frac{P(N_{ij}^{\text{obs}}, N_{ij}^{\text{exp}})}{P(N_{ij}^{\text{obs}}, N_{ij}^{\text{obs}})} \\ &= 2 \sum_{i,j} \left(N_{ij}^{\text{exp}} - N_{ij}^{\text{obs}} + N_{ij}^{\text{obs}} \times \ln \frac{N_{ij}^{\text{obs}}}{N_{ij}^{\text{exp}}} \right) \end{aligned} \quad (6)$$

where $P(n, \nu) = \nu^n e^{-\nu} / n!$ is the Poisson probability of finding n events with a expectation value ν , N_{ij}^{obs} and N_{ij}^{exp} are the observed and expected number of events in the i -th Q^2 bin in subsample j ($j = \text{one track}, \mu + p, \mu + \pi$ with high and low vertex activity), respectively. The expected number of events for each sample is given by:

$$N_{i, 1\text{trk}}^{\text{exp}} = R_{\text{norm}} \cdot \left[n_{i,1\text{trk}}^{\text{QE}} + R_{\text{res}} n_{i,1\text{trk}}^{\text{res}} + R_{\text{other}} n_{i,1\text{trk}}^{\text{other}} \right] \quad (7)$$

$$N_{i, \mu p}^{\text{exp}} = R_{\text{norm}} \cdot R_{2\text{trk}/1\text{trk}} \cdot R_{p/\pi} \cdot \left[n_{i,\mu p}^{\text{QE}} + R_{\text{res}} n_{i,\mu p}^{\text{res}} + R_{\text{other}} n_{i,\mu p}^{\text{other}} \right] \quad (8)$$

$$N_{i, \mu\pi\text{H}}^{\text{exp}} = R_{\text{norm}} \cdot R_{2\text{trk}/1\text{trk}} \cdot \left[n_{i,\mu\pi\text{H}}^{\text{QE}} + R_{\text{res}} n_{i,\mu\pi\text{H}}^{\text{res}} + R_{\text{other}} n_{i,\mu\pi\text{H}}^{\text{other}} \right] \quad (9)$$

$$N_{i, \mu\pi\text{L}}^{\text{exp}} = R_{\text{norm}} \cdot R_{2\text{trk}/1\text{trk}} \cdot R_{\text{act}} \cdot \left[n_{i,\mu\pi\text{L}}^{\text{QE}} + R_{\text{res}} n_{i,\mu\pi\text{L}}^{\text{res}} + R_{\text{other}} n_{i,\mu\pi\text{L}}^{\text{other}} \right] \quad (10)$$

where $n_{i,j}^{\text{QE}}$, $n_{i,j}^{\text{res}}$, $n_{i,j}^{\text{other}}$ are the number of charged current quasi-elastic, charged current resonant pion, and other events in each bin in each subsample, respectively. R_{pscale} and κ do not appear explicitly in these equations, but R_{pscale} causes migration between Q^2 bins and κ changes $n_{i,j}^{\text{QE}}$.

The term χ_{sys}^2 , added to constrain systematic parameters, is calculated as:

$$\chi_{\text{sys}}^2 = (\mathbf{P}_{\text{sys}} - \mathbf{P}_0) \mathbf{V}^{-1} (\mathbf{P}_{\text{sys}} - \mathbf{P}_0) \quad (11)$$

where \mathbf{P}_{sys} represents the set of systematic parameters and \mathbf{P}_0 is the set of parameter values before fitting, expressed as:

$$\mathbf{P}_{\text{sys}} = \begin{pmatrix} R_{\text{res}} \\ R_{2\text{trk}/1\text{trk}} \\ R_{p/\pi} \\ R_{\text{pscale}} \end{pmatrix}, \quad \mathbf{P}_0 = \begin{pmatrix} 1 \\ 1 \\ 1 \\ 1 \end{pmatrix}. \quad (12)$$

\mathbf{V} is a covariance matrix estimated by considering the possible variations due to systematic uncertainties in the detector responses, nuclear effects, neutrino interaction models, and neutrino beam spectrum. We prepare several MC event sets by changing each underlying physics parameter, i.e. the source of systematic uncertainty, by $\pm 1\sigma$. The covariance between two systematic parameters p_i and p_j is calculated as:

$$V_{ij} \equiv \text{cov}[p_i, p_j] = \sum_{\text{source}} \frac{\Delta p_i \Delta p_j|_+ + \Delta p_i \Delta p_j|_-}{2} \quad (13)$$

where $\Delta p_i \Delta p_j|_{+(-)}$ is the product of variations of two parameters when the underlying physics parameter is increased (decreased) by the size of its uncertainty. The covariance matrix is estimated to be:

$$\mathbf{V} = \begin{pmatrix} (0.20)^2 & -(0.09)^2 & +(0.10)^2 & 0 \\ -(0.09)^2 & (0.09)^2 & -(0.07)^2 & 0 \\ +(0.10)^2 & -(0.07)^2 & (0.15)^2 & 0 \\ 0 & 0 & 0 & (0.02)^2 \end{pmatrix}. \quad (14)$$

R_{norm} , R_{other} , R_{act} , and κ are unconstrained in the fit.

Events with $Q_{\text{rec}}^2 < 0.10$ (GeV/c)² in the $\mu + \pi$ sample with low activity are not included in the fit to avoid charged current coherent pion signal events. A data excess is observed in the region with $Q_{\text{rec}}^2 < 0.15$ (GeV/c)² in the $\mu + p$ sample. Further investigation reveals that the second track in the excess events is emitted at a relatively large angle with respect to the beam direction and has large dE/dx , thus the events have an additional large energy deposition at the vertex. Each of these events seems to have a muon and a proton with additional activity, and therefore the excess is not expected to affect the charged current coherent pion analysis. A possible candidate for the excess is charged current resonant pion production where the pion is absorbed in the nucleus. In such an event, two or more additional nucleons should be emitted after the pion is absorbed, which is currently not simulated. The excess cannot be explained with the introduced fitting parameters, and therefore the region is not used in the fit.

Fig. 10 shows reconstructed Q^2 after the fitting for the one track, $\mu + p$, and $\mu + \pi$ events with and without vertex activity. The best fit values and errors of the fit parameters are summarized in Table II. These same

fit parameters are also applied to the MRD penetrating sample. The $\chi^2/\text{d.o.f}$ before the fit is $473/75 = 6.31$. The $\chi^2/\text{d.o.f}$ after the fit is $117/67 = 1.75$. Even after fitting, the reduced χ^2 is relatively large, which indicates that the introduced parameters are not sufficient in fully reproducing the data. To take into account the incompleteness of our simulation, we enlarge the errors on the fitting parameters by a factor of $\sqrt{\chi^2/\text{d.o.f}}$.

TABLE II: Best fit values and errors of the fitting parameters

| Parameter | Value | Error |
|-------------------------------|-------|-------|
| R_{norm} | 1.103 | 0.029 |
| $R_{2\text{trk}/1\text{trk}}$ | 0.865 | 0.035 |
| $R_{p/\pi}$ | 0.899 | 0.038 |
| R_{act} | 0.983 | 0.055 |
| R_{pscale} | 1.033 | 0.002 |
| R_{res} | 1.211 | 0.133 |
| R_{other} | 1.270 | 0.148 |
| κ | 1.019 | 0.004 |

F. Charged Current Coherent Pion Event Selection

Charged current coherent pion candidates are extracted from both the MRD stopped and MRD penetrated samples with the same selection criteria. In this section, we describe the event selection for the MRD stopped sample. The event selection for the MRD penetrated sample is summarized later.

After selecting $\mu + \pi$ events which do not have vertex activity, the sample still contains charged current quasi-elastic events in which a proton is misidentified as a minimum ionizing track. We reduce this charged current quasi-elastic background by making use of kinematic information in the event. Since the charged current quasi-elastic interaction is a two-body interaction, one can predict the proton direction from the measured muon momentum p_μ and muon angle θ_μ ;

$$\vec{p}_p = (-p_{\mu x}, -p_{\mu y}, E_\nu^{\text{rec}} - p_\mu \cos \theta_\mu) \quad (15)$$

where $p_{\mu x}$ and $p_{\mu y}$ are the projected muon momentum in the x and y dimension, respectively. E_ν^{rec} is the reconstructed neutrino energy given by Equation 4. For each two-track event, we define an angle called $\Delta\theta_p$ as the angle between the expected proton track direction given by Equation 15 and the observed second track direction. Fig. 11 shows the $\Delta\theta_p$ distribution for $\mu + \pi$ events in the MRD stopped sample. Events with $\Delta\theta_p$ larger than 20 degrees are selected. With this selection, 48% of charged current quasi-elastic events in the $\mu + \pi$ sample are rejected, while 91% of charged current coherent pion events pass the cut according to the MC simulation.

Further selections are applied in order to separate charged current coherent pion events from charged cur-

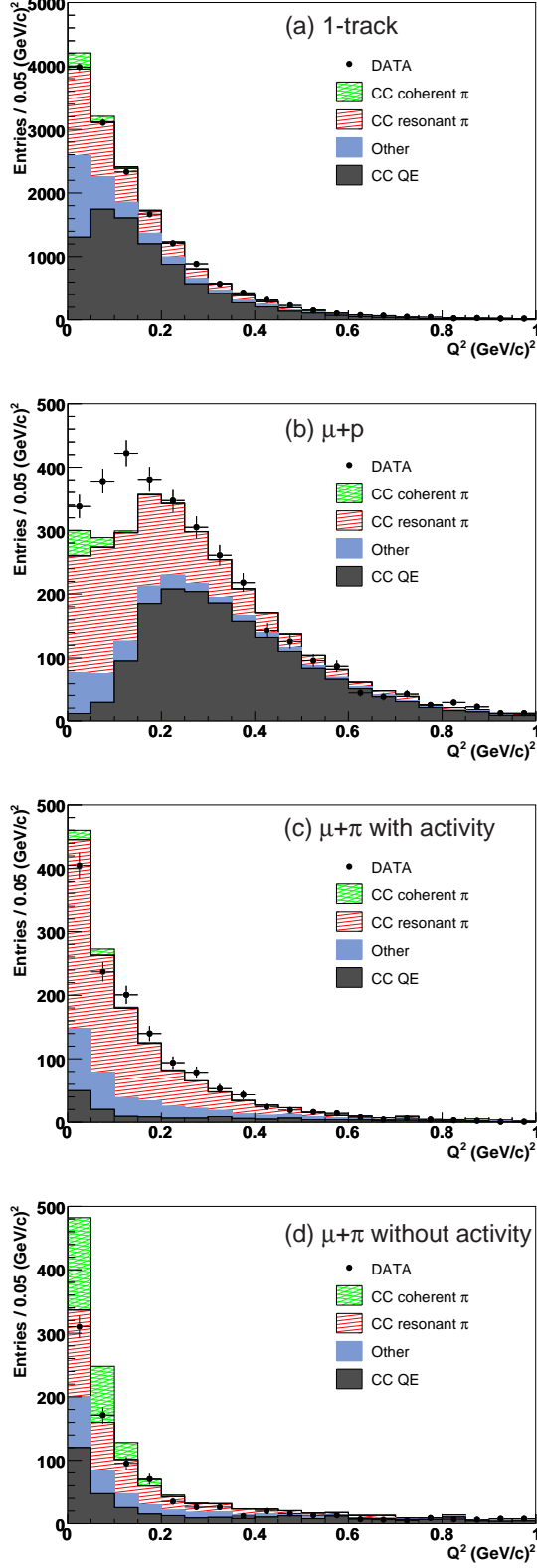


FIG. 10: (Color online) Reconstructed Q^2 after fitting for (a) the one track, (b) $\mu + p$, (c) $\mu + \pi$ with activity, and (d) $\mu + \pi$ without activity samples.

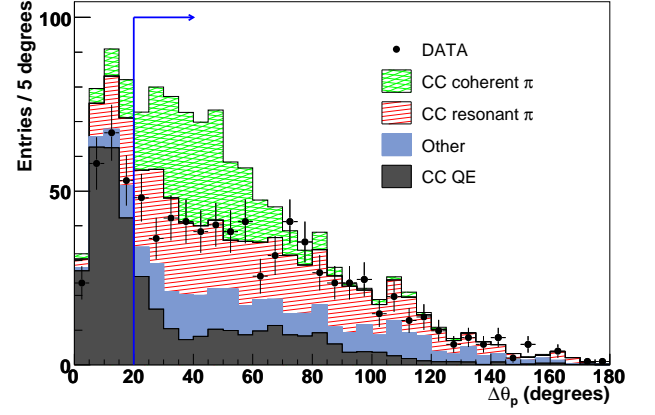


FIG. 11: (Color online) $\Delta\theta_p$ for the $\mu + \pi$ events in the MRD stopped sample after fitting.

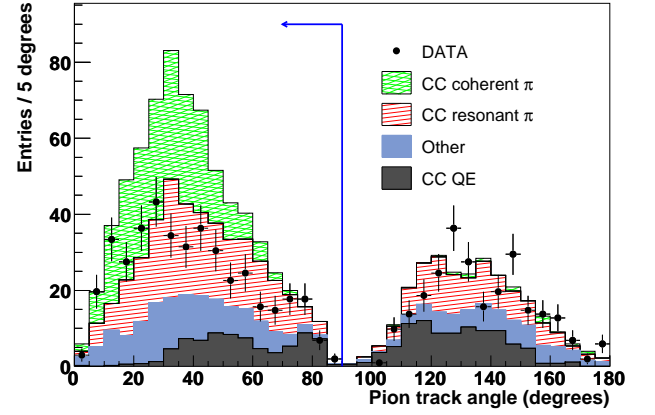


FIG. 12: (Color online) Track angle of the pion candidate with respect to the beam direction for the $\mu + \pi$ events after the charged current quasi-elastic rejection after fitting.

rent resonant pion events which are the dominant backgrounds for this analysis. Fig. 12 shows the angular distribution of pion candidates with respect to the beam direction. In the case of charged current coherent pion events, both the muon and pion tracks are directed forward. Events in which the track angle of the pion candidate with respect to the beam direction is less than 90 degrees are selected.

Fig. 13 shows the reconstructed Q^2 distribution for the $\mu + \pi$ events after the pion track direction cut. Although a charged current quasi-elastic interaction is assumed, the Q^2 of charged current coherent pion events is reconstructed with a resolution of $0.016 (\text{GeV}/c)^2$ and a shift of $-0.024 (\text{GeV}/c)^2$ according to the MC simulation. Finally, events with reconstructed Q^2 less than $0.1 (\text{GeV}/c)^2$ are selected. The charged current coherent pion event selection is summarized in Table III. In the

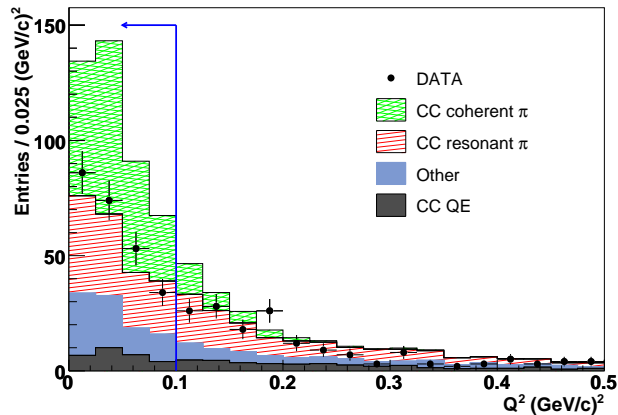


FIG. 13: (Color online) Reconstructed Q^2 for the $\mu + \pi$ events in the MRD stopped sample after the pion track direction cut and after fitting.

TABLE III: Event selection summary for the MRD stopped charged current coherent pion sample.

| Event selection | DATA | MC | | Coherent π Efficiency |
|------------------------------|--------|--------|---------|------------------------------|
| | | Signal | B.G. | |
| Generated in SciBar fid.vol. | | 1,939 | 156,766 | 100% |
| SciBar-MRD matched | 30,337 | 978 | 29,359 | 50.4% |
| MRD stopped | 21,762 | 715 | 20,437 | 36.9% |
| 2 track | 5,939 | 358 | 6,073 | 18.5% |
| Particle ID ($\mu + \pi$) | 2,255 | 292 | 2,336 | 15.1% |
| Vertex activity cut | 887 | 264 | 961 | 13.6% |
| CC-QE rejection | 682 | 241 | 709 | 12.4% |
| Pion track direction cut | 425 | 233 | 451 | 12.0% |
| Reconstructed Q^2 cut | 247 | 201 | 228 | 10.4% |

signal region, 247 charged current coherent pion candidates are observed, while the expected number of background events is 228 ± 12 . The error comes from the errors on the fitting parameters summarized in Table II. The background in the final sample is dominated by charged current resonant pion production. The “other” background is comprised of 50% charged current DIS, 32% neutral current, and 18% $\bar{\nu}_\mu$ events. The selection efficiency for the signal is estimated to be 10.4%.

G. MRD penetrated Charged Current Coherent Pion Events

The same selection is applied to the MRD penetrated sample to extract charged current coherent pion candidates at higher energy. Fig. 14 shows the reconstructed Q^2 distribution of the MRD penetrated charged current coherent pion sample. The reconstructed Q^2 and E_ν for the MRD penetrated sample are calculated from

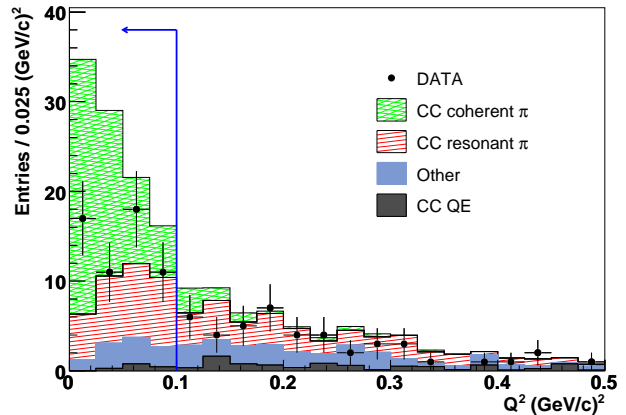


FIG. 14: (Color online) Reconstructed Q^2 for the $\mu + \pi$ events in the MRD penetrated sample after the pion track direction cut after fitting.

TABLE IV: Event selection summary of MRD penetrated charged current coherent pion sample.

| Event selection | DATA | MC | | Coherent π Efficiency |
|------------------------------|--------|--------|---------|------------------------------|
| | | Signal | B.G. | |
| Generated in SciBar fid.vol. | | 1,939 | 156,766 | 100% |
| SciBar-MRD matched | 30,337 | 978 | 29,359 | 50.4% |
| MRD penetrated | 3,712 | 177 | 4,375 | 9.1% |
| 2 track | 1,029 | 92 | 1,304 | 4.7% |
| Particle ID ($\mu + \pi$) | 418 | 78 | 474 | 4.0% |
| Vertex activity cut | 167 | 71 | 186 | 3.6% |
| CC-QE rejection | 134 | 67 | 135 | 3.5% |
| Pion track direction cut | 107 | 66 | 109 | 3.4% |
| Reconstructed Q^2 cut | 57 | 60 | 40 | 3.1% |

muon angle and partially-reconstructed muon energy, using Equation 3 and Equation 4, respectively. Although only a part of the muon energy is observed, the Q^2 reconstruction performance is essentially same because of the small muon angle. The event selection is summarized in Table IV. In the signal region, 57 charged current coherent pion candidates are observed, while the expected number of background events is 40 ± 2.2 . The background in the final sample is dominated by charged current resonant pion production. The “other” background is comprised of 75% charged current DIS, and 25% $\bar{\nu}_\mu$ events. The selection efficiency for the signal is estimated to be 3.1%.

VII. RESULTS

A. Cross Section Ratio

1. MRD stopped charged current coherent pion sample

After subtracting background and correcting for the selection efficiency, the number of charged current coherent pion candidates in the MRD-stopped sample is measured to be $179 \pm 190(\text{stat})$; this error includes the uncertainty in the background estimation. No evidence of charged current coherent pion production is found in the sample. The neutrino energy dependence of the selection efficiency for charged current coherent pion events is shown in Fig. 15. The mean neutrino beam energy for true charged current coherent pion events in the sample is estimated to be 1.1 GeV after accounting for the effects of the selection efficiency. The RMS of the neutrino beam energy is 0.27 GeV.

The total number of charged current interactions is estimated by using the SciBar-MRD matched sample. We observe 30,337 SciBar-MRD matched events. As described in section VI, the selection efficiency and purity of charged current events are estimated to be 27.9% and 92.8%, respectively. The neutrino energy dependence of the selection efficiency for charged current events is shown in Fig. 16. After correcting for the efficiency and purity, the number of charged current events is measured to be $(1.091 \pm 0.006(\text{stat})) \times 10^5$.

Using this information, the ratio of the charged current coherent pion to total charged current production cross sections is measured to be $(0.16 \pm 0.17(\text{stat})_{-0.27}^{+0.30}(\text{sys})) \times 10^{-2}$ at 1.1 GeV, where the systematic error is described later. The result is consistent with the non-existence of charged current coherent pion production, and hence we set an upper limit on the cross section ratio by using the likelihood distribution (\mathcal{L}) which is convolved with the systematic error. We calculate the 90% confidence level (C.L.) upper limit (UL) using the relation $\int_0^{\text{UL}} \mathcal{L} dx / \int_0^{\infty} \mathcal{L} dx = 0.9$ to be:

$$\frac{\sigma(\text{CC coherent } \pi)}{\sigma(\text{CC})} < 0.67 \times 10^{-2} \quad (16)$$

at a mean neutrino energy of 1.1 GeV.

2. MRD penetrated charged current coherent pion sample

After subtracting background and correcting for the selection efficiency, the number of charged current coherent pion candidates in the MRD penetrating sample is measured to be $548 \pm 254(\text{stat})$. As in the MRD stopping sample, this includes the uncertainty due to the background estimation. The mean neutrino beam energy for true charged current coherent pion events in the sample is estimated to be 2.2 GeV after accounting for the ef-

fects of the selection efficiency. The RMS of the neutrino beam energy is 0.80 GeV.

Due to the higher neutrino energy in the charged current coherent pion sample, the MRD penetrated charged current sample is chosen to estimate the number of total charged current interactions at a similar neutrino energy. We observe 3,712 MRD penetrated events, and the efficiency and purity of true ν_μ charged current events are estimated to be 4.5% and 97.5%, respectively. The impurity largely comes from $\bar{\nu}_\mu$ charged current events. After correcting the efficiency and purity, the number of charged current events is measured to be $(0.804 \pm 0.013(\text{stat})) \times 10^5$. A 26% difference between the MRD matched and penetrated samples is found while the estimated uncertainty due to the neutrino flux is 14%. However, this is expected to be a small effect on the cross section ratio measurement.

The ratio of the charged current coherent pion to total charged current production cross sections is measured to be $(0.68 \pm 0.32(\text{stat})_{-0.25}^{+0.39}(\text{sys})) \times 10^{-2}$ at 2.2 GeV. The systematic error is described later. No significant evidence for charged current coherent pion production is observed, and hence we set an upper limit on the cross section ratio at 90% C.L.:

$$\frac{\sigma(\text{CC coherent } \pi)}{\sigma(\text{CC})} < 1.36 \times 10^{-2} \quad (17)$$

at a mean neutrino energy of 2.2 GeV.

B. Systematic Uncertainties

The sources of systematic error are divided into five categories, (i) detector response and track reconstruction, (ii) nuclear effects, (iii) neutrino interaction models, (iv) neutrino beam, and (v) event selection. We vary these sources within their uncertainties and take the resulting change in the cross section ratio as the systematic uncertainty of the measurement. Table V summarizes the uncertainties in the charged current coherent pion cross section ratio for the MRD stopped and MRD penetrated samples. The total systematic error is $_{-0.27}^{+0.30} \times 10^{-2}$ for the MRD stopped sample, and $_{-0.25}^{+0.39} \times 10^{-2}$ for the MRD penetrated sample.

1. Detector Response and Track Reconstruction

The crosstalk of the MA-PMT was measured to be 3.15% for adjacent channels, with an absolute error of 0.4%. The single photoelectron resolution of the MA-PMT is set to 50% in the simulation, to reproduce the observed dE/dx distribution of cosmic muons. The absolute error is estimated to be $\pm 20\%$. Birk's constant of the SciBar scintillator was measured to be 0.0208 \pm 0.0023 cm/MeV [51] and is varied within the measurement error to evaluate the systematic. The hit threshold for track reconstruction is varied by $\pm 20\%$.

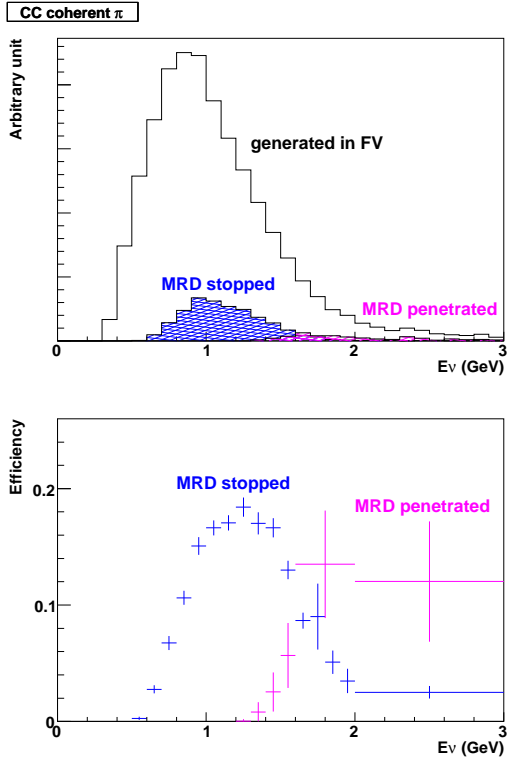


FIG. 15: (Color online) Neutrino energy spectra and selection efficiencies as a function of neutrino energy for charged current coherent pion events.

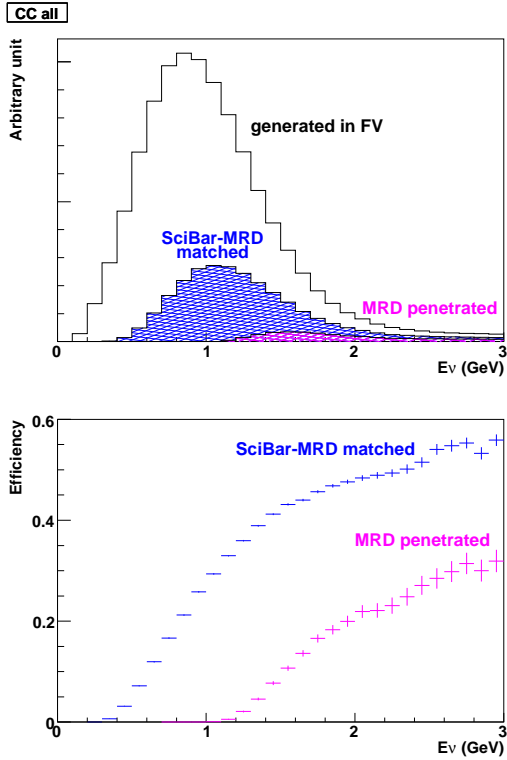


FIG. 16: (Color online) Neutrino energy spectra and selection efficiencies as a function of neutrino energy for all charged current events.

TABLE V: Summary of the systematic errors in the charged current coherent pion cross section ratio.

| Source | MRD stopped error ($\times 10^{-2}$) | | MRD penetrated error ($\times 10^{-2}$) | |
|----------------------------|---|-------|--|-------|
| Detector response | +0.10 | -0.18 | +0.18 | -0.18 |
| Nuclear effect | +0.20 | -0.07 | +0.19 | -0.09 |
| Neutrino interaction model | +0.17 | -0.04 | +0.08 | -0.04 |
| Neutrino beam | +0.07 | -0.11 | +0.27 | -0.13 |
| Event selection | +0.07 | -0.14 | +0.06 | -0.05 |
| Total | +0.30 | -0.27 | +0.39 | -0.25 |

2. Nuclear Effects

We consider uncertainties in final state interactions inside the nucleus. This includes rescattering of nucleons and pions in the initial target nucleus. For pions produced by neutrino interactions, uncertainties on the cross sections for pion absorption and pion inelastic scattering in the nucleus are considered. The cross section of pion charge exchange is negligible compared with the other effects and is hence neglected. In the momentum range of pions from Δ decays, the cross section measurement uncertainty for both absorption and inelastic scattering is approximately 30% [44]. Nucleon re-scattering in the nucleus affects vertex activity. The uncertainty in the cross section is estimated to be 10%. In the NEUT simulation, the Fermi momentum of nucleons is set to 217 MeV/c for carbon. According to electron quasi-elastic scattering data [54], the value is approximately 221 ± 5 MeV/c. Therefore, an uncertainty of ± 5 MeV/c is assigned.

3. Neutrino Interaction Models

In the NEUT simulation, we set the axial vector mass M_A to 1.21 GeV/c² for both QE and resonant pion production. The uncertainty in this value is estimated to be approximately ± 0.1 GeV/c² based on recent measurements [31, 32]; results from past experiments are systematically lower than the recent measurements [55], and thus we only vary M_A to 1.11 GeV/c², and take that change as the systematic error. We consider the uncertainty in the charged current resonant $\mu^- n \pi^+ / \mu^- p \pi^+$ cross section ratio. The uncertainty in this ratio is estimated to be 7% using four SciBooNE data samples described in Section VID. In addition, a disagreement of the Q^2 shape is observed in the $\mu + \pi$ events with vertex activity where charged current resonant pion production is dominant, as shown in Fig. 10. We estimate the systematic uncertainty, due to evident low Q^2 suppression of charged current resonant pion production even after the MC tuning, by re-weighting the true Q^2 distribution of charged current resonant pion events according to the observed low Q^2 deficit.

4. Neutrino Beam

The uncertainties in secondary particle production cross sections in proton-beryllium (p-Be) interactions, hadronic interactions in the target or horn, and the horn magnetic field model are varied within their externally estimated error bands. Detailed descriptions of each uncertainty are found elsewhere [24]. Uncertainties associated with the delivery of the primary proton beam to the beryllium target and the primary beam optics, which result in the overall normalization uncertainty, are not considered in this analysis since it cancels in the cross section ratio.

5. Event Selection

For the event selection variable $\Delta\theta_p$, we evaluate the systematic uncertainty in the cross section ratio by varying the cut placement. The uncertainty in the $\Delta\theta_p$ cut for charged current quasi-elastic rejection is estimated to be ± 5 degrees. For the other variables, we already tuned the MC simulation using the migration parameters or considered possible systematic sources. Therefore, we do not include additional systematic uncertainties due to these selections.

C. Discussion

Having not observed evidence for charged current coherent pion production, we set 90% C.L. upper limits at two different mean neutrino energies. According to the Rein-Sehgal model [5, 8] implemented in our simulation, the cross section ratio of charged current coherent pion production to total charged current interactions is expected to be 2.04×10^{-2} . Our limits correspond to 33% and 67% of the prediction at 1.1 GeV and 2.2 GeV, respectively. For reference, the total charged current cross section averaged over the MRD stopped and MRD penetrated samples are 1.05×10^{-38} cm²/nucleon and 1.76×10^{-38} cm²/nucleon, respectively, estimated with the MC simulation. Our results are consistent with the K2K result; $\sigma(\text{CC coherent } \pi)/\sigma(\text{CC}) < 0.60 \times 10^{-2}$ at 90% C.L. measured in a 1.3 GeV wide-band neutrino beam. As shown in Fig. 2, several recent models predict a considerably smaller coherent cross section, which appears consistent with our results.

Because of the connection of the neutrino and antineutrino coherent pion production processes in the theoretical models, it will be interesting to repeat this analysis on SciBooNE's already collected antineutrino data. Most models predict a similar absolute cross section for neutrino and antineutrino coherent pion production, which means the ratio of charged current coherent pion events to charged current inclusive events is expected to be

larger in antineutrino data because of the reduced total $\bar{\nu}$ charged current event rate. Because of this, the antineutrino search has the potential to be even more sensitive.

Furthermore, theoretical models also make concrete connections between the charged and neutral current coherent pion production processes. As mentioned in Section I, the MiniBooNE Collaboration has already published an observation of neutral current coherent pion production in the same neutrino beam as SciBooNE. The SciBooNE neutral current coherent pion search is, therefore, also interesting and may shed considerable light on the behavior of this interaction process.

VIII. CONCLUSIONS

In conclusion, we have searched for muon neutrino charged current coherent pion production on carbon in the few GeV region using the full SciBooNE neutrino data set of 0.99×10^{20} protons on target. No evidence of charged current coherent pion production is found, and hence we set 90% C.L. upper limits on the cross section ratio of charged current coherent pion to total charged current production cross sections at 0.67×10^{-2} and 1.36×10^{-2} , at mean neutrino energies of 1.1 GeV and 2.2 GeV, respectively.

IX. ACKNOWLEDGMENTS

The SciBooNE Collaboration sincerely expresses our gratitude to Prof. Yoji Totsuka who helped us to start this experiment. We acknowledge the Physics Department at Chonnam National University, Dongshin University, and Seoul National University for the loan of parts used in SciBar and the help in the assembly of SciBar. We wish to thank the Physics Departments at the University of Rochester and Kansas State University for the loan of Hamamatsu PMTs used in the MRD. We gratefully acknowledge support from Fermilab as well as various grants, contracts and fellowships from the MEXT and JSPS (Japan), the INFN (Italy), the Ministry of Science and Innovation and CSIC (Spain), the STFC (UK), and the DOE and NSF (USA). This work was supported by MEXT and JSPS with the Grant-in-Aid for Scientific Research A 19204026, Young Scientists S 20674004, Young Scientists B 18740145, Scientific Research on Priority Areas “New Developments of Flavor Physics”, and the global COE program “The Next Generation of Physics, Spun from Universality and Emergence”. The project was supported by the Japan/U.S. Cooperation Program in the field of High Energy Physics and by JSPS and NSF under the Japan-U.S. Cooperative Science Program. K. H. would like to acknowledge support from JSPS.

-
- [1] Y. Itow, Nucl. Phys. Proc. Suppl. **112**, 3 (2002).
- [2] D. A. Harris *et al.* [MINERvA Collaboration], arXiv:hep-ex/0410005.
- [3] S. L. Adler, Phys. Rev. **135**, B963 (1964).
- [4] S. S. Gershtein, Yu. Y. Komachenko, and M. Y. Khlopov, Sov. J. Nucl. Phys. **32**, 861 (1980) [Yad. Fiz. **32**, 1663 (1980)].
- [5] D. Rein and L. M. Sehgal, Nucl. Phys. B **223**, 29 (1983).
- [6] A. A. Belkov and B. Z. Kopeliovich, Sov. J. Nucl. Phys. **46**, 499 (1987) [Yad. Fiz. **46**, 874 (1987)].
- [7] E. A. Paschos, A. Kartavtsev, and G. J. Gounaris, Phys. Rev. D **74**, 054007 (2006) [arXiv:hep-ph/0512139].
- [8] D. Rein and L. M. Sehgal, Phys. Lett. B **657**, 207 (2007) [arXiv:hep-ph/0606185].
- [9] S. K. Singh, M. Sajjad Athar, and S. Ahmad, Phys. Rev. Lett. **96**, 241801 (2006).
- [10] L. Alvarez-Ruso, L. S. Geng, S. Hirenzaki, and M. J. Vicente Vacas, Phys. Rev. C **75**, 055501 (2007) [arXiv:nucl-th/0701098].
- [11] L. Alvarez-Ruso, L. S. Geng, and M. J. Vicente Vacas, Phys. Rev. C **76**, 068501 (2007) [arXiv:0707.2172 [nucl-th]].
- [12] J. E. Amaro, E. Hernandez, J. Nieves and M. Valverde, arXiv:0811.1421 [hep-ph].
- [13] M. Hasegawa *et al.* [K2K Collaboration], Phys. Rev. Lett. **95**, 252301 (2005) [arXiv:hep-ex/0506008].
- [14] H. Faissner *et al.*, Phys. Lett. B **125**, 230 (1983).
- [15] E. Isiksal, D. Rein, and J. G. Morfin, Phys. Rev. Lett. **52**, 1096 (1984).
- [16] A. A. Aguilar-Arevalo *et al.* [MiniBooNE Collaboration], Phys. Lett. B **664**, 41 (2008) [arXiv:0803.3423 [hep-ex]].
- [17] H. J. Grabosch *et al.* [SKAT Collaboration], Z. Phys. C **31**, 203 (1986).
- [18] P. Vilain *et al.* [CHARM-II Collaboration], Phys. Lett. B **313**, 267 (1993).
- [19] P. Marage *et al.* [BEBC WA59 COLLABORATION Collaboration], Z. Phys. C **31**, 191 (1986).
- [20] P. P. Allport *et al.* [BEBC WA59 Collaboration], Z. Phys. C **43**, 523 (1989).
- [21] S. Willocq *et al.* [E632 Collaboration], Phys. Rev. D **47**, 2661 (1993).
- [22] A. A. Aguilar-Arevalo *et al.* [SciBooNE Collaboration], arXiv:hep-ex/0601022.
- [23] S. Agostinelli *et al.* [GEANT4 Collaboration], Nucl. Instrum. Meth. A **506**, 250 (2003).
- [24] A. A. Aguilar-Arevalo *et al.* [MiniBooNE Collaboration], arXiv:0806.1449 [hep-ex].
- [25] M. G. Catanesi *et al.*, Eur. Phys. J. C **52**, 29 (2007) [arXiv:hep-ex/0702024].
- [26] I. Chemakin *et al.* [E910 Collaboration], Phys. Rev. C **77**, 015209 (2008) [Erratum-ibid. C **77**, 049903 (2008)] [arXiv:0707.2375 [nucl-ex]].
- [27] Y. Hayato, Nucl. Phys. Proc. Suppl. **112**, 171 (2002).
- [28] G. Mitsuka, AIP Conf. Proc. **981**, 262 (2008).
- [29] C. H. Llewellyn Smith, Phys. Rept. **3**, 261 (1972).
- [30] R. A. Smith and E. J. Moniz, Nucl. Phys. B **43**, 605 (1972) [Erratum-ibid. B **101**, 547 (1975)].
- [31] R. Gran *et al.* [K2K Collaboration], Phys. Rev. D **74**, 052002 (2006) [arXiv:hep-ex/0603034].
- [32] A. A. Aguilar-Arevalo *et al.* [MiniBooNE Collaboration], Phys. Rev. Lett. **100**, 032301 (2008) [arXiv:0706.0926 [hep-ex]].
- [33] D. Rein and L. M. Sehgal, Annals Phys. **133**, 79 (1981).
- [34] C. Berger and L. M. Sehgal, Phys. Rev. D **76**, 113004 (2007) [arXiv:0709.4378 [hep-ph]].
- [35] K. S. Kuzmin, V. V. Lyubushkin, and V. A. Naumov, Mod. Phys. Lett. A **19**, 2815 (2004) [Phys. Part. Nucl. **35**, S133 (2004)] [arXiv:hep-ph/0312107].
- [36] D. Rein, Z. Phys. C **35**, 43 (1987).
- [37] T. Kitagaki *et al.*, Phys. Rev. D **34**, 2554 (1986).
- [38] S. K. Singh, M. J. Vicente-Vacas, and E. Oset, Phys. Lett. B **416**, 23 (1998) [Erratum-ibid. B **423**, 428 (1998)].
- [39] M. Gluck, E. Reya, and A. Vogt, Eur. Phys. J. C **5**, 461 (1998) [arXiv:hep-ph/9806404].
- [40] A. Bodek and U. K. Yang, arXiv:hep-ex/0308007.
- [41] M. Nakahata *et al.* [KAMIOKANDE Collaboration], J. Phys. Soc. Jap. **55**, 3786 (1986).
- [42] T. Sjostrand, Comput. Phys. Commun. **82**, 74 (1994).
- [43] L. L. Salcedo, E. Oset, M. J. Vicente-Vacas, and C. Garcia-Recio, Nucl. Phys. A **484**, 557 (1988).
- [44] D. Ashery, I. Navon, G. Azuelos, H. K. Walter, H. J. Pfeiffer, and F. W. Schlegel, Phys. Rev. C **23**, 2173 (1981).
- [45] G. Rowe, M. Salomon, and R. H. Landau, Phys. Rev. C **18**, 584 (1978).
- [46] K. Nitta *et al.*, Nucl. Instrum. Meth. A **535** (2004) 147 [arXiv:hep-ex/0406023].
- [47] M. Yoshida *et al.*, IEEE Trans. Nucl. Sci. **51** (2004) 3043.
- [48] S. Buontempo *et al.*, Nucl. Instrum. Meth. A **349** (1994) 70.
- [49] A. Heikkinen, N. Stepanov, and J. P. Wellisch, *In the Proceedings of 2003 Conference for Computing in High-Energy and Nuclear Physics (CHEP 03), La Jolla, California, 24-28 Mar 2003, pp MOMT008* [arXiv:nucl-th/0306008].
- [50] J. Birks, *Theory and Practice of Scintillation Counting*, Pergamon Press, 1964.
- [51] M. Hasegawa, Ph.D. thesis, Kyoto University, 2006.
- [52] H. Maesaka, Ph.D. thesis, Kyoto University, 2005.
- [53] S. Baker and R. D. Cousins, Nucl. Instrum. Meth. **221**, 437 (1984).
- [54] E. J. Moniz, I. Sick, R. R. Whitney, J. R. Ficenc, R. D. Kephart, and W. P. Trower, Phys. Rev. Lett. **26**, 445 (1971).
- [55] V. Bernard, L. Elouadrhiri, and U. G. Meissner, J. Phys. G **28**, R1 (2002) [arXiv:hep-ph/0107088].